Preliminary results obtained with the ZEUS phasing sensor within the APE experiment

I. Surdej[a], B. Luong[c], A. Vigan[b], C. Araujo[a], R. Bourtembourg[a], R. Brast[a], P. Duhoux[a], C. Dupuy[a], C. Frank[a], F. Gonte[a], R. Karban[a], R. Mazzoleni[a], L. Noethe[a], N. Yaitskova[a], K. Dohlen[b]

[a] European Organisation for Astronomical Research in the Southern Hemisphere, Karl-Schwarzschild-Str. 2, Garching, Germany
[b]Laboratoire d′Astrophysique de Marseille, B.P. 8, F-13376 Marseille Cedex 12, France
[c]FOGALE nanotech, 125 rue de l′Hostellerie, 30900 Nimes, France

ABSTRACT

In the framework of the Active Phasing Experiment (APE), four different phasing techniques are tested. The ZErnike Unit for Segment phasing sensor (ZEUS) is integrated on the APE bench. APE has been tested in the laboratory before it will be installed on one of the Nasmyth platform of a Very Large Telescope (VLT) Unit Telescope to perform on sky tests. The ZEUS phasing sensor concept has its origins in the Mach-Zehnder interferometer equipped with a spatial filter in its focal plane. In this paper, the ZEUS phasing sensor is described together with its theoretical background and deployment within the APE experiment. The algorithms and its elements used to reconstruct the wavefront are described. Finally, the preliminary results obtained in the laboratory are presented.

Keywords: Telescope, Segmentation, Phasing, ELT, ZEUS

1. INTRODUCTION

The purpose of the Active Phasing Experiment (APE),[1] designed at the European Southern Observatory (ESO), is to validate phasing strategies for Extremely Large Telescopes (ELTs). The experiment is currently in a laboratory at ESO, Garching. At the end of the year 2008, APE will be in Paranal to be tested on sky on a Nasmyth platform of a Unit Telescope of the Very Large Telescope (VLT).
Four different phasing sensors will be tested on the APE bench: a Shack-Hartmann Phasing Sensor (SHAPS) developed by ESO,[2] a Diffraction Image Phase Sensing Instrument developed by Instituto de Astrofisica de Canarias, a Pyramid Phasing Sensor developed by Arcetri Astrophysical Observatory and the ZErnike Unit for Segment phasing (ZEUS) developed by Laboratoire d′Astrophysique de Marseille.
A segmented mirror of 61 hexagons is conjugated to the primary mirror of the VLT.[3] The segments are controlled in piston, tip and tilt by means of an internal metrology system developed by Fogale.[4] The precision of the internal metrology system is less than 1 nm RMS.
The experiment is currently tested in the laboratory and preliminary results have been obtained for the SHAPS and the ZEUS sensors. The first results obtained with the ZEUS sensor are based on images without atmospheric turbulence. However, in the very near future atmospheric turbulence will be simulated in the laboratory.
In section 2 the concept of the ZEUS sensor is explained and the analytical expression of the signal is studied. The signal analysis algorithm developed is explained in section 3. In section 4, the preliminary results obtained with the ZEUS sensor on images acquired in the APE laboratory are presented. The effects of gaps, phase mask de-centering and edge effects are for the first time observed on real data.

Further author information: (Send correspondence to Isabelle Surdej.)
E-mail: isurdej@eso.org, Telephone: 0049 89 3200 6452

Ground-based and Airborne Telescopes II, edited by Larry M. Stepp, Roberto Gilmozzi,
Proc. of SPIE Vol. 7012, 701218, (2008) · 0277-786X/08/$18 · doi: 10.1117/12.789689

Downloaded from SPIE Digital Library on 10 Jan 2012 to 134.171.34.17. Terms of Use: http://spiedl.org/terms

2. OVERVIEW OF THE ZEUS PHASING SENSOR

2.1 Concept

The concept of the ZEUS sensor is based on the Mach-Zehnder interferometer.[5] A pinhole is placed in one arm of the Mach-Zehnder interferometer as illustrated on fig. 1. When its diameter is of the order of the seeing disk, it

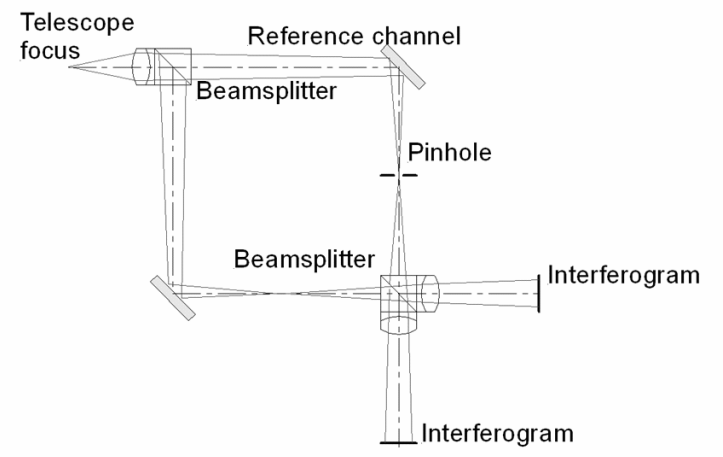

Figure 1. Mach-Zehnder interferometer layout.

partially filters out the wavefront aberrations generated by atmospheric turbulence. Atmospheric turbulence has a power spectral density which is dominated by low spatial frequencies whereas segmentation errors have strong high frequency components. With the appropriate size of the pinhole, the lower frequencies interfere destructively and the interferogram will mainly reveal the high frequencies of the incoming wave, which correspond to the segment misalignments. In the ZEUS sensor, the pinhole of the interferometer is replaced, as in the Zernike

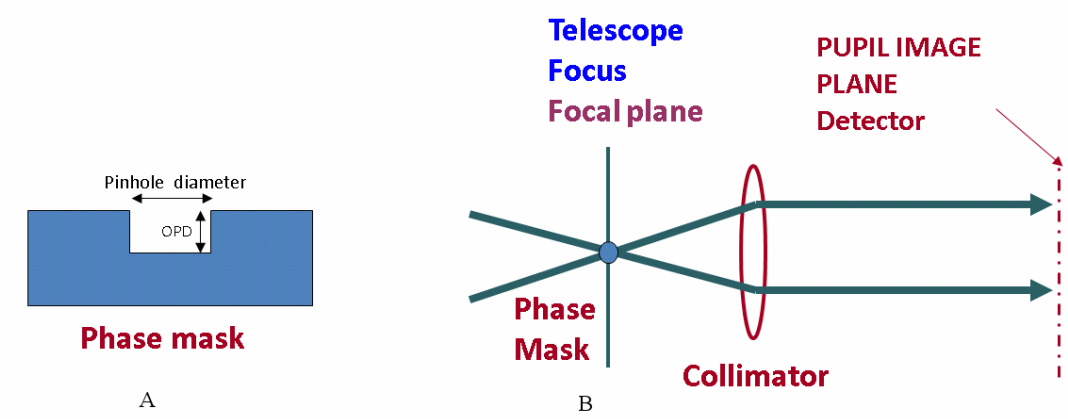

Figure 2. *A*: ZEUS phase mask. *B*: ZEUS sensor layout.

phase contrast method, with a circular phase mask.[6] The phase mask consists of a cylindrical pellet etched within a substrate with a certain depth corresponding to a chosen phase difference (referred to as Optical Path Difference, OPD) and with a diameter of the order of the seeing disk, as illustrated on fig. 2 *A*.
Fig. 2 *B* shows schematically the layout of the ZEUS sensor. A detector is placed in the pupil image plane where the output interferogram is recorded, fig. 3 *A*. The signals are intensity profiles perpendicular to the segment edges.
In this article only the piston errors are considered, that is, the segments are assumed to be perfectly aligned in

Downloaded from SPIE Digital Library on 10 Jan 2012 to 134.171.34.17. Terms of Use: http://spiedl.org/terms

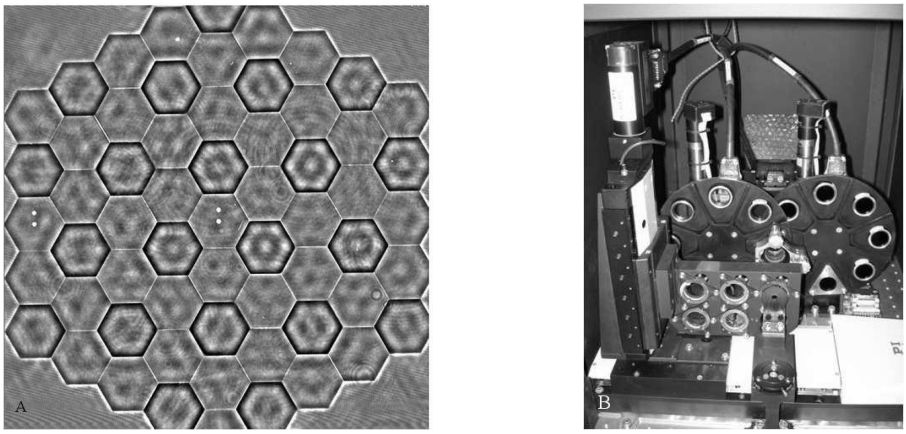

Figure 3. *A*: ZEUS output interferogram at 880 nm with 1" pinhole and 175nm OPD. *B*: ZEUS integrated on the APE bench.

tip and tilt.
Fig. 3 *B* shows the ZEUS sensor integrated on the APE bench.

2.2 Theoretical treatment

Three different images are required to obtain the normalized signal image I_S : the interferogram I with the phase mask located at the focus, an image with the phase mask translated such that the focus does not pass through the cylindrical pellet of the phase mask but only through the substrate (reference image I_R), and a dark frame I_D obtained by covering the light path to obtain information on dark noise. The normalized signal image is then defined as:

$$I_S = \frac{I - I_R}{I_R - I_D} \tag{1}$$

A deep theoretical study has been done for the Mach-Zehnder interferometer.[5] Most of these results are also applicable to the ZEUS sensor, the theoretical signals having very similar expressions (eq. 2 and eq. 3). The analytical expression of the intensity profiles perpendicular to the segment edges for the Mach-Zehnder interferometer (eq. 2) and for the ZEUS sensor[6] (eq. 3) in the signal image I_s, have the following analytical expressions respectively :

$$S_{\mathrm{MZ}}(x) \quad = \quad (1 - f(b|x|))\mathrm{sign}(x)\sin(\varphi_0)\sin(\Delta\varphi) \tag{2}$$

$$S_{\mathrm{Z}}(x) = -\{1 - f(b|x|)\}\{f(b|x|)(1-\cos(\varphi_0))(1-\cos(\Delta\varphi)) - \mathrm{sign}(x)\sin(\varphi_0)\sin(\Delta\varphi)\}, \tag{3}$$

where x is the axis perpendicular to the segment border, φ_0 is the optical path difference, b is related to the pinhole diameter a expressed in arcsecond by $b = \pi a/\lambda$, and $\Delta\varphi = \frac{2\pi}{\lambda}\Delta p$, with Δp being the physical piston step. $f(b|x|)$ is the *normalized sine integral*:

$$f(bx) = \frac{2}{\pi}\mathrm{Si}(bx) = \frac{2}{\pi}\int_0^{bx}\frac{\sin(t)}{t}dt. \tag{4}$$

In the case of the ZEUS sensor (eq. 3) the signal is the sum of two terms, one symmetric and one antisymmetric, as illustrated on fig. 4:

- Symmetric term: $\quad -\{1 - f(b|x|)\}f(b|x|)$
- Antisymmetric term: $\quad \{1 - f(b|x|)\}\mathrm{sign}(x)$

The antisymmetric term is the same as the Mach-Zehnder signal (eq. 2). The shape of the signal is related to the piston difference Δp. It is a periodic function of $\Delta\varphi$, and the range of the measurable phase difference

Downloaded from SPIE Digital Library on 10 Jan 2012 to 134.171.34.17. Terms of Use: http://spiedl.org/terms

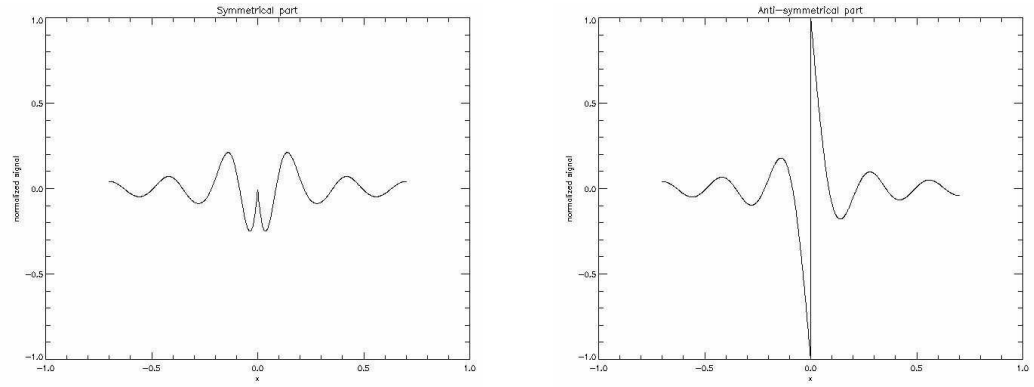

Figure 4. Symmetrical and antisymmetrical parts of the signal

is therefore limited to $[-\pi, \pi]$, with a 2π ambiguity. The Mach-Zehnder interferometer is limited to the range $[-\pi/2, \pi/2]$, since there is no symmetrical part in the signal, and therefore has a π ambiguity.
Fig. 6 shows the ZEUS signal shape for different piston steps.
When the phase is in the range $[0 \dots \pi/2[$ the antisymmetrical part of the signal dominates, whereas in the range $[\pi/2 \dots \pi[$, the symmetrical part of the signal dominates.

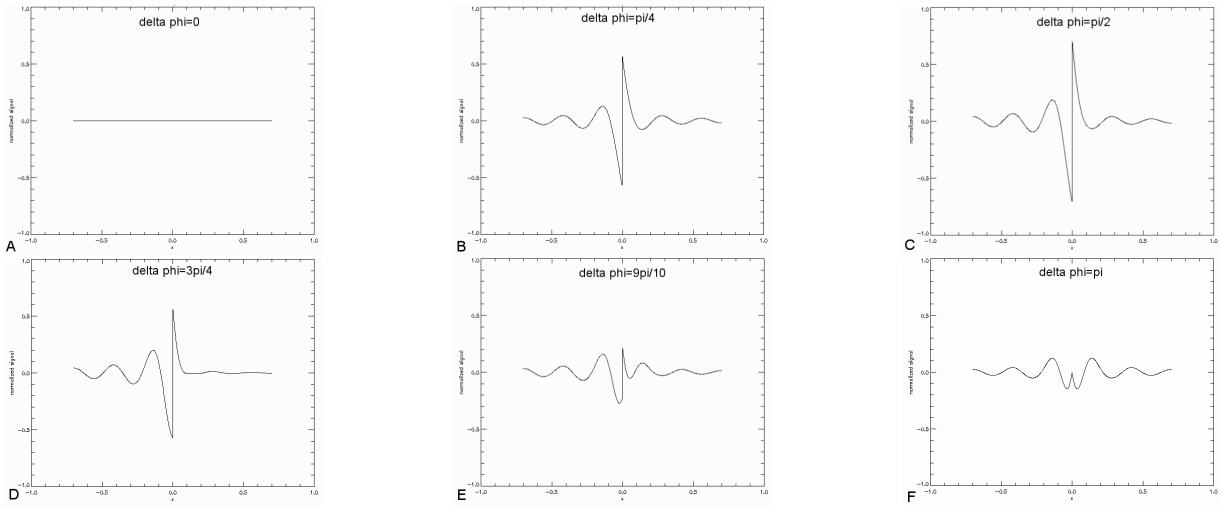

Figure 5. Signal profiles for an OPD of $\frac{\pi}{4}$ and for different $\Delta\varphi$ ranging from 0 to π. A: $\Delta\varphi = 0$, B: $\Delta\varphi = \pi/4$, C: $\Delta\varphi = \pi/2$, D: $\Delta\varphi = 3\pi/4$, E: $\Delta\varphi = 9\pi/10$, F: $\Delta\varphi = \pi$. The abscissa x is the axis perpendicular to the border, $x = 0$ represents the segment edge.

2.2.1 Signal width

The b parameter appearing in eq. 2 and 3 is proportional to the pinhole diameter, expressed by a, and inversely proportional to the wavelength, expressed by λ:

$$b = \frac{\pi a}{\lambda} \tag{5}$$

This parameter determines the width of the signal, Δx, illustrated in fig. 2.2.1. If the signal width is defined as the distance between the two first zeroes of the curve, it can be expressed in pixels as:

$$\Delta x[pixels] = \frac{253.5 \quad \lambda/[nm] \quad e^{-6}}{a/[arcsec] \quad grid/[mm]} \tag{6}$$

Downloaded from SPIE Digital Library on 10 Jan 2012 to 134.171.34.17. Terms of Use: http://spiedl.org/terms

where *grid* is defined as the pixel size in *mm*.
From eq. 6, the signal width is proportional to the wavelength and inversely proportional to the pinhole size.

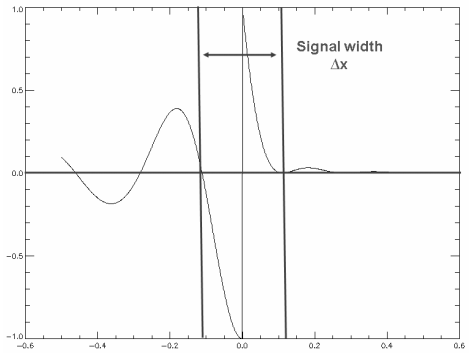

Figure 6. Illustration of the definition of the signal width

3. SIGNAL ANALYSIS

In the following sections, all the steps required to retrieve the phase steps related to the misalignments of the segments from the ZEUS sensor images are described.

3.1 Pattern recognition and signal extraction

A precise knowledge of the position and orientation of the border in the image is required to extract the one-dimensional signal profiles. A robust pattern recognition algorithm is used to automatically retrieve the center of the image, the hexagon size and the orientation of the hexagonal pattern.[7]
After the pattern recognition, the locations of the segment edges are known with sufficient precision to extract the one-dimensional signal profiles. The signals are averaged over the segment borders in order to increase the signal to noise ratio. The signals are then extracted from a two-dimensional window centered on the hexagon border, fig. 7 *a*. The projection along the axis perpendicular to the edge results in the expected profile described by eq. 3 (see fig. 7 *b*).

3.2 Signal analysis algorithm

A fitting algorithm is used to determine the piston steps at the segment edges. The theoretically expected signal of eq. 3 can be expressed as a function of the piston step and a few other nuisance parameters. A theoretically derived function with a few open parameters is fitted to the data. The fitting process will determine the

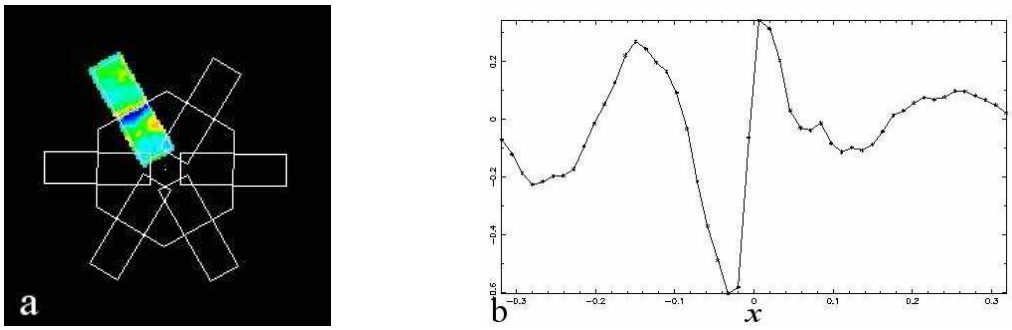

Figure 7. *a* : ZEUS two-dimensional signal within a chosen sub-aperture centered on the segment border from which the signal is extracted. *b* : Two-dimensional signal projected on the axis perpendicular to the border.

Downloaded from SPIE Digital Library on 10 Jan 2012 to 134.171.34.17. Terms of Use: http://spiedl.org/terms

parameters for which the function fits the signal best in the least squares sense.
Expressing the theoretical equation of the signal (eq. 3) as a function of the fitted parameters, results in the following formula :

$$S(x) = a_3 + [1 - f(a_5|x - a_4|)]\{a_2 f(a_5|x - a_4|)(1 - \cos(\varphi_0)) - a_1 sign(x - a_4)\sin(\varphi_0)\} \quad (7)$$

The five free parameters are:

- a_1: Proportional to the sine $\sin(\Delta\varphi)$ of the phase $\Delta\varphi$ of the piston step
- a_2: Proportional to the cosine $\cos(\Delta\varphi)$ of the phase $\Delta\varphi$ of the piston step
- a_3: Constant background
- a_4: Shift of the edge with respect to the position $x = 0$
- a_5: Related to the parameter b, which is inversely proportional to the width of the signal

The function $S(x)$ is fitted in the least squares sense to the data describing the measured intensities profiles perpendicular to the segment edges. The piston step is then deduced from the parameters a_1 and a_2 which are proportional to the sine and cosine of the piston step respectively:

$$a_1 = C\sin(\Delta\varphi) = C\sin(\frac{2\pi}{\lambda}\Delta p) \quad (8)$$

$$a_2 = C\cos(\Delta\varphi) = C\cos(\frac{2\pi}{\lambda}\Delta p) \quad (9)$$

where C depends on external parameters such as the atmosphere. Eq. 8 and 9 are called *calibration curves*.

4. PRELIMINARY RESULTS WITH ZEUS LABORATORY IMAGES

In this section, the preliminary results obtained with ZEUS laboratory images are presented. Images obtained with the sensor in simulation and in the laboratory are first shown and compared.

4.1 ZEUS simulated images and laboratory images

The right column of fig. 8 shows four CCD signal images acquired with the ZEUS sensor on the APE bench and their corresponding simulated images processed in identical conditions in the left column. The segmented mirror is in the same configuration for all the images. Each row corresponds to a different phase mask and wavelength configuration.
The simulated images and the laboratory images show very similar signals. Due to the gaps between the segments of the APE segmented mirror (ASM) all segments are visible on the laboratory images.

4.2 ZEUS signal profiles

Fig. 9 shows some ZEUS signal profiles extracted from the normalized signal image I_s together with the fitted curve for four different piston steps (PS) at different wavelengths and with different phase masks.
It proves that all the experimental data can be fitted using eq. 7. The agreement between the experimental data and the theoretical expression validates the theoretical background outlined in section 2.2.
It also clearly shows that the width of the signal as defined in section 2.2.1 depends on the wavelength and the pinhole size, verifying the relation expressed by eq. 6.

Downloaded from SPIE Digital Library on 10 Jan 2012 to 134.171.34.17. Terms of Use: http://spiedl.org/terms

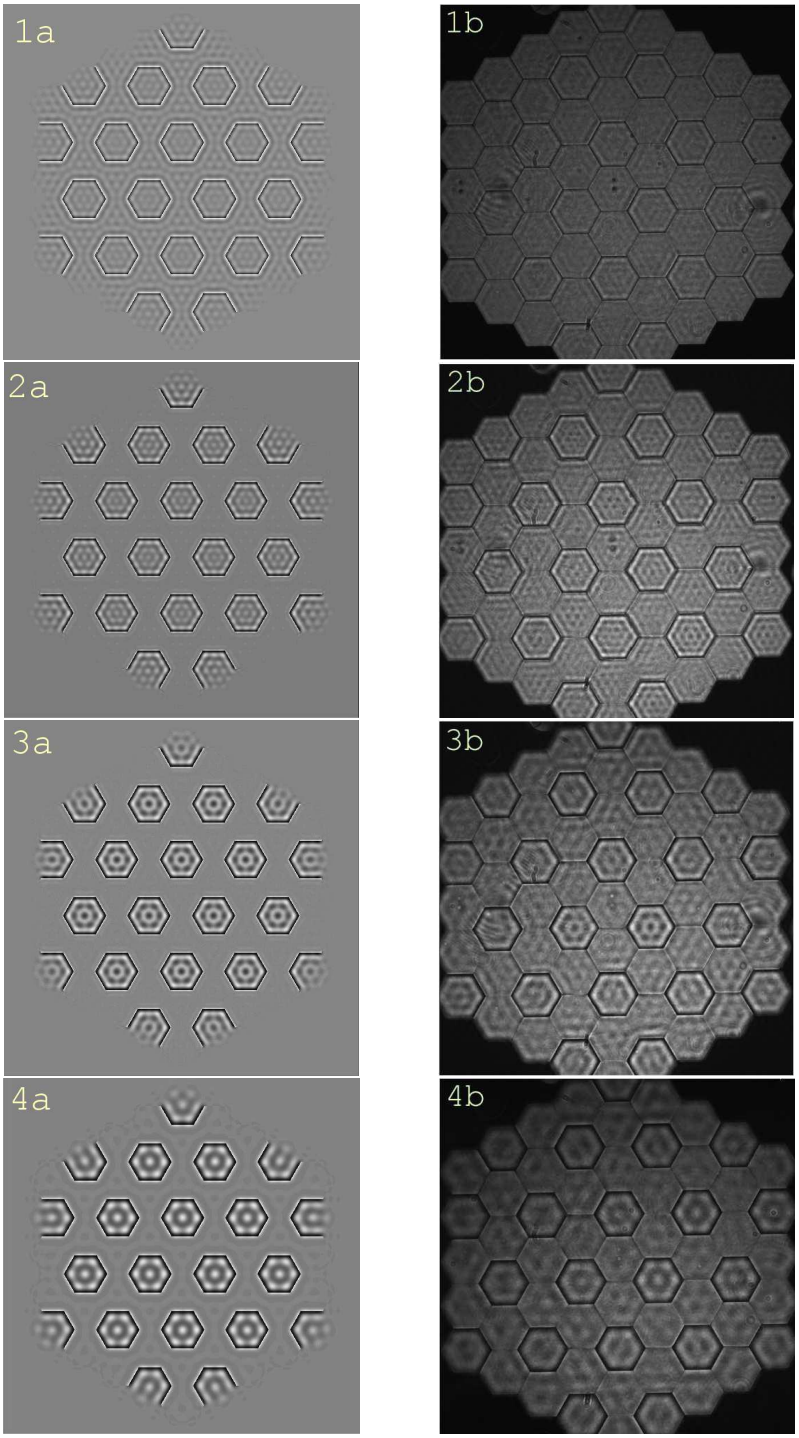

Figure 8. The left column (a) contains four different ZEUS simulated interferogram images. The right column (b) contains four laboratory ZEUS interferogram images. The configuration of the ASM is identical for all images. One family of segments is pushed by a physical step of $\lambda/8$. Each row corresponds to a different configuration of wavelengths and phase masks. *row* 1: $\lambda = 650nm$, pinhole diameter=1.5", OPD = 100nm. *row* 2: $\lambda = 650nm$ pinhole diameter=1.5", OPD = 175nm. *row* 3: $\lambda = 650nm$ pinhole diameter=1", OPD = 175nm. *row* 4: $\lambda = 880nm$ pinhole diameter=1", OPD = 175nm.

Downloaded from SPIE Digital Library on 10 Jan 2012 to 134.171.34.17. Terms of Use: http://spiedl.org/terms

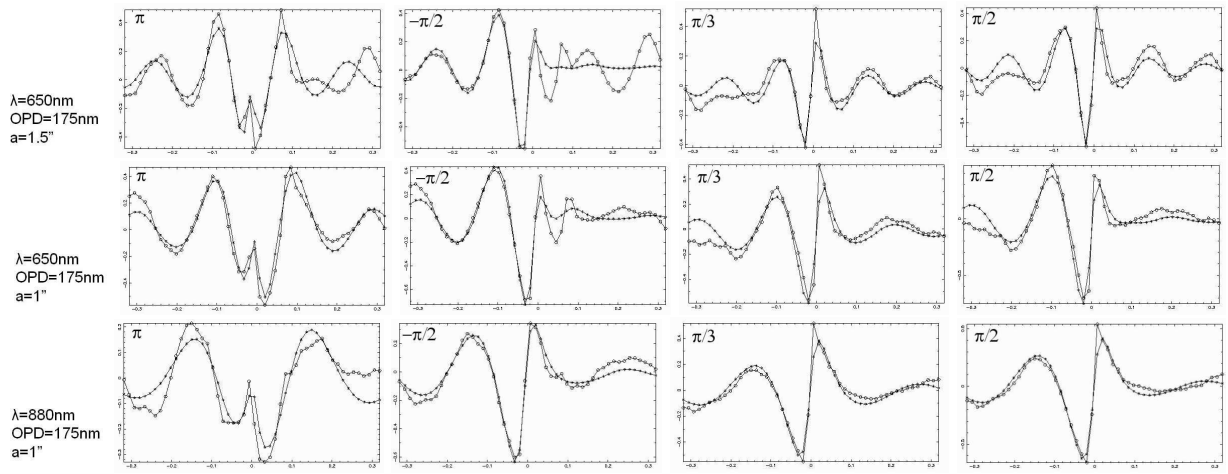

Figure 9. Signal profiles (circles) and fitted curves (cross) for different phase masks and wavelengths. *col* 1: PS = π, *col* 2: PS = $-\pi/2$, *col* 3: PS = $\pi/3$, *col* 4: PS = $\pi/2$

4.3 Image analysis

In this section, it is studied if the parameters a_1 and a_2 obtained by the fitting of eq. 7 to the experimental data can be used for an accurate determination of the piston steps (PS).
There are three families of segments on the segmented mirror. These are segments with non common borders as illustrated on fig. 10.
A set of 41 images has been acquired by changing the piston of a family of segments from $-\lambda/4$ to $+\lambda/4$ with physical steps of $\lambda/80$. The positions of the segments of the ASM can be controlled in piston by an internal metrology system. All the 41 images are then analyzed and the fitted parameters are plotted for each border as a function of the piston applied on the segmented mirror. By doing so, two calibration curves (eq. 8 and 9) per border are obtained.

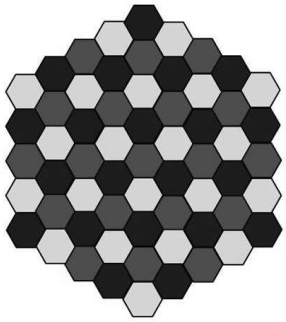

Figure 10. Three families of segments.

Fig. 11 illustrates the calibration curves for three different borders from images obtained in different configurations of phase masks and wavelengths. The calibration curves are plotted for the two fitted parameters a_1 (left column) and a_2 (right column) as a function of the applied wavefront piston step. These curves are compared to the theoretical sine curve for a_1 and cosine curve for a_2.
The performance of the ZEUS sensor is better when using a smaller pinhole or a larger wavelength. This is due to the fact that the width of the signal is larger for smaller pinholes and bigger wavelengths. A larger signal width results in a better sampling of the signal and thus leads to a better fitting of the data. However, in the presence of atmospherical turbulence, the size of the pinhole is limited by the seeing conditions.

Downloaded from SPIE Digital Library on 10 Jan 2012 to 134.171.34.17. Terms of Use: http://spiedl.org/terms

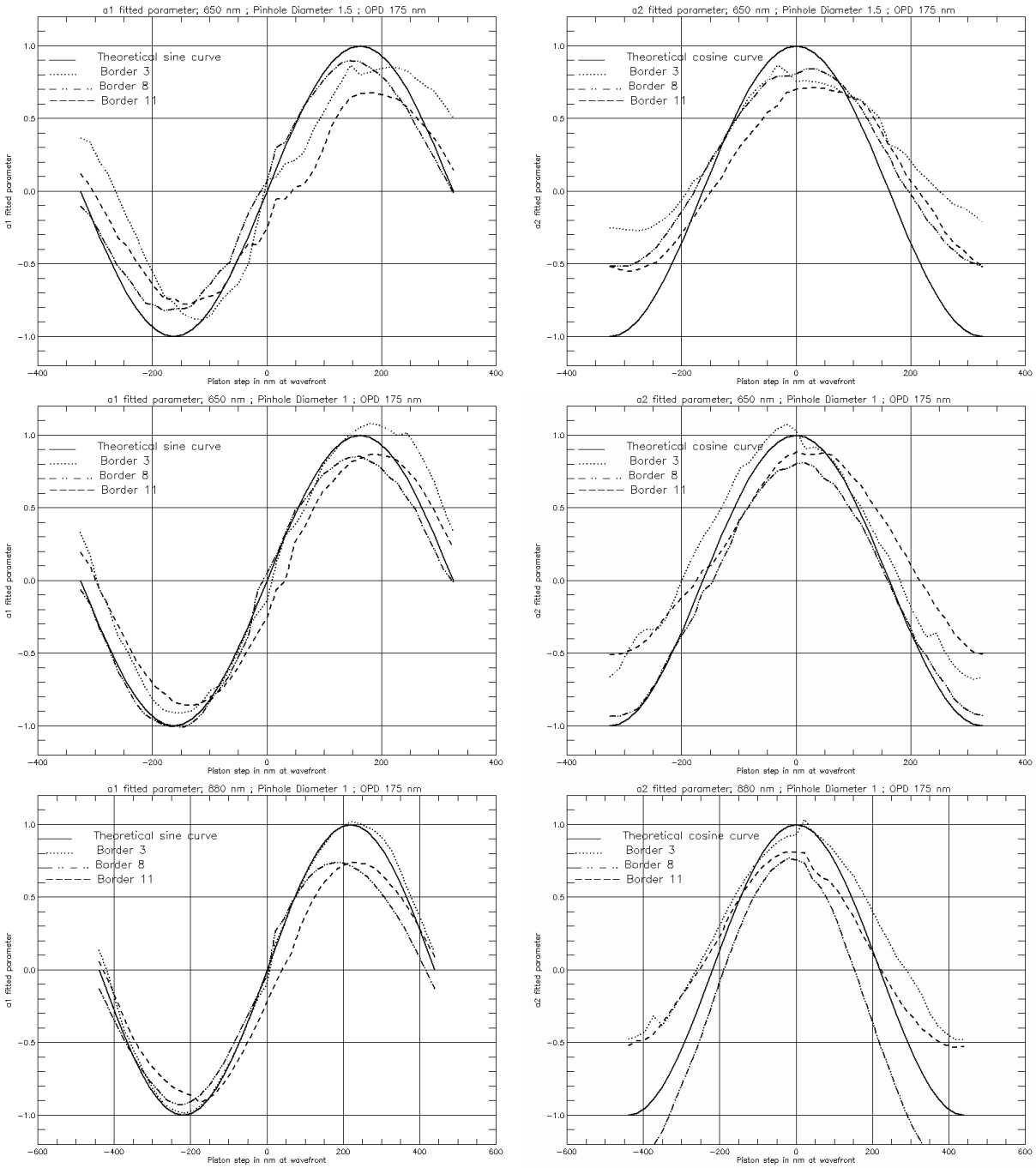

Figure 11. Calibration curves of the ZEUS sensor for different borders at different wavelengths and with different phase masks. *row* 1 : 650nm, a=1.5", OPD = 175nm; *row* 2 : 650nm, a=1", OPD = 175nm; *row* 3 : 880nm, a=1", OPD = 175nm

Downloaded from SPIE Digital Library on 10 Jan 2012 to 134.171.34.17. Terms of Use: http://spiedl.org/terms

Fig. 11 shows a relatively good matching between the theoretical sine and cosine curves and the experimental data. However, on all plots, one can observe three main discrepancies:

- horizontal offset of the calibration curves
- vertical offset of the calibration curves
- change in the scale of the calibration curves

These discrepancies can be expressed by modifying eq. 8 and 9 with the following expressions :

$$a_1 = A\sin(\Delta\varphi + \varphi_1) + B \quad (10)$$

$$a_2 = C\cos(\Delta\varphi + \varphi_2) + D \quad (11)$$

where φ_1 and φ_2 represent the horizontal offset, B and D represent the vertical offset and A and C represent the changes in scale. At this stage of the experiment, these effects could not be deeply analyzed yet. However, in the next section, some preliminary qualitative explanations are presented based on a theoretical study developed by Yaitskova *et al.*[5] for the Mach-Zehnder interferometer. There are residual polishing errors appearing near the edges of the segments. As explained previously, the information about the piston steps for the ZEUS sensor is located at the inter-segment edge. These residual polishing errors generate a piston signal even when the segmented mirror is phased. The presence of residual polishing errors modify the calibration curves: they introduce a horizontal offset, expressed by the parameters φ_1 and φ_2.
Furthermore, a misalignment of the system generates a vertical offset of the calibration curves, expressed by the parameters B and D. It includes a shift of the phase mask with respect to the central peak of the point-spread function. This effect will be studied in the future on the APE bench.
An additional effect is the presence of gaps between the segments which modifies the shape of the signal and decreases the signal's amplitude. The presence of atmosphere also decreases the signal's amplitude as well as the width of the signal. The decrease in amplitude is expressed by the parameters A and C (A and C are smaller than 1).
Thus, all these effects result in a significant discrepancy between the theoretical curve and the experimental data. Therefore, it is necessary to calibrate the segmented mirror in order to determine the piston steps accurately.

4.4 Calibration

In the APE experiment, different calibration techniques are going to be tested.[8] The first idea that comes to mind to calibrate an entire segmented mirror is to determine experimentally the calibration curves for every border between every single segment, such as performed here above. However, since the calibration curves depend on various external parameters (wavelength, seeing conditions, etc.), in practice, they would require to be determined before each observation. This is one important reason why this so-called *global calibration* approach cannot be applied for future large telescopes with many segments*.
An improvement of the *global calibration* approach is the so-called *local calibration*. In this approach, it is assumed that all borders have the same calibration curves. A calibration curve is experimentally determined for one segment border and used for the entire segmented mirror. However, the resulting calibration curves still depend on external parameters such as seeing conditions and they need to be determined at the beginning of the observing night. This problem could be resolved with a *synthetic calibration*. In this approach, the calibration curves are not determined experimentally, but predicted from theory or from simulations. Therefore, the parameters A, B, C, D, φ_1 and φ_2 need to be calculated with a theoretical expression or determined with simulations for different seeing conditions, wavelengths, etc. This will be the subject of future studies in the framework of APE.
Using any of these three calibration techniques, the parameters introduced in eq. 10 and 11 can be determined to finally measure the piston step.

$$\Delta p = \frac{\lambda}{2\pi}[\arcsin(\frac{a_1 - B}{A}) - \varphi_1] \quad (12)$$

$$\Delta p = \frac{\lambda}{2\pi}[\arccos(\frac{a_2 - D}{C}) - \varphi_2] \quad (13)$$

*ESO is currently working on a European-Extremely large telescope (E-ELT) whith 984 segments.

Downloaded from SPIE Digital Library on 10 Jan 2012 to 134.171.34.17. Terms of Use: http://spiedl.org/terms

The last step of the phasing algorithm consists of converting the relative piston steps between segment borders to segment absolute pistons. The rigid-body movements of the segment, which minimize the overall RMS of the phasing errors, are calculated from the measured phase steps across the edges with the help of an inverted matrix derived by Singular Value Decomposition.[9]

5. CONCLUSION

The ZEUS sensor has been successfully integrated on the APE bench in order to test the phasing of segmented mirrors for future ELTs. The first ZEUS laboratory images obtained are in agreement with the theoretical analyzes and simulations. The signal profiles extracted from the images are very similar to the theoretically expected signals. These results demonstrate that the implemented fitting algorithm is well adapted to the analysis of the ZEUS signal.
Furthermore, the calibration curves were determined experimentally for different configurations and compared with the theoretical curves. A very good agreement between theory and experimental data was demonstrated. However, some discrepancies due to external effects such as edge effects, phase mask de-centering or gaps were observed. In the future, these discrepancies will have to be analyzed. The most efficient calibration procedure will be investigated in order to retrieve accurately the phase steps at the inter-segment borders.
The effect of the atmosphere on the ZEUS sensor will also be analyzed using a turbulence generator placed on the APE bench in future experiments.

ACKNOWLEDGMENTS

This project forms part of the ELT Design Study and is supported by the European Commission, within Framework Programme 6, contract No 011863.
We would like to thank Silvio Mazzanti, Maud Langlois and Marc Ferrari for all the help to obtain these results.

REFERENCES

1. F. Gonte, R. Karban, R. Mazzoleni, and L. Noethe, "Active Phasing Experiment: preliminary results," in *Ground-based and Airborne Telescopes*, *Proc. SPIE* **7012-34**, 2008.
2. R. Mazzoleni and all, "Design and performances of the Shack-Hartmann sensor within the active phasing experiment," in *Ground-based and Airborne Telescopes*, *Proc. SPIE* **7012-124**, 2008.
3. C. Dupuy, C. Frank, and F. Gonte, "ASM: a scaled-down Active Segmented Mirror for the Active Phasing Experiment," in *Ground-based and Airborne Telescopes*, *Proc. SPIE* **7012-127**, 2008.
4. R. C. Wilhelm, B. Luong, A. Courteville, S. Estival, and F. Gonte, "Optical phasing of a segmented mirror with subnanometer accuracy: experimental results of the APE Internal Metrology," in *Ground-based and Airborne Telescopes*, *Proc. SPIE* **7012-37**, 2008.
5. N. Yaitskova, K. Dohlen, P. Dierickx, and L. Montoya, "Mach-zehnder interferometer for piston and tip-tilt sensing in segmented telescopes: theory and analytical treatment," *Optical Society of America* **22**, pp. 1093–1105, 2005.
6. K. Dohlen, M. Langlois, P. Lanzoni, S. Mazzanti, L. Montoya, M. Reyes, I. Surdej, and N. Yaitskova, "ZEUS, a cophasing sensor based on the Zernike phase contrast method," in *Ground-based and Airborne Telescopes*, L. Stepp, ed., *Proc. SPIE* **6267-132**, 2006.
7. I. Surdej, H. Lorch, L. Noethe, N. Yaitskova, and R. Karban, "Pattern recognition and signal analysis in a Mach-Zehnder type phasing sensor," *Proc. SPIE* **6696**, 2007.
8. N. Yaitskova and al, "The Active Phasing Experiment Part I: Concept and Objectives," in *Ground-based and Airborne Telescopes*, L. Stepp, ed., *Proc. SPIE* **6267-84**, 2006.
9. G. Chanan, C. Ohara, and M. Troy, "Phasing the mirror segments of the Keck telescopes II: the narrow-band phasing algorithm," *Appl. Opt.* **39**, pp. 4706–4714, 2000.

Downloaded from SPIE Digital Library on 10 Jan 2012 to 134.171.34.17. Terms of Use: http://spiedl.org/terms